DOI: 10.1002/marc.((insert number)) ((or ppap., mabi., macp., mame., mren., mats.))

Full paper

RAFT emulsion polymerisation as a platform to generate well-defined biocompatible latex nanoparticles.

Pratik Gurnani, Carlos Sanchez-Cano, Kristin Abraham, Helena Xandri-Monje, Alexander B. Cook, Matthias Hartlieb, Francis Lévi, Robert Dallmann, Sébastien Perrier*

_____

P. Gurnani, Dr C. Sanchez-Cano, A.B. Cook, Dr M. Hartlieb, Prof. S.Perrier
Department of Chemistry, University of Warwick, Gibbet Hill Road, Coventry, CV4 7AL, UK

E-mail: s.perrier@warwick.ac.uk

K. Abraham, H. Xandri-Monje, Prof. F. Lévi, Dr R. Dallmann, Prof. S. Perrier
Warwick Medical School, University of Warwick, Gibbet Hill Road, Coventry, CV4 7AL, UK

Prof. S. Perrier
Faculty of Pharmacy and Pharmaceutical Sciences, Monash University, 381 Royal Parade, Parkville, VIC 3052, Australia.
_____

Abstract:

Current approaches to generate core-shell nanoparticles for biomedical applications are limited by factors such as synthetic scalability and circulatory desorption of cytotoxic surfactants. Developments in controlled radical polymerisation, particularly in dispersed states, represent a promising method of overcoming these challenges. In this work, well-defined PEGylated nanoparticles were synthesised using reversible addition fragmentation chain transfer emulsion polymerisation to control particle size and surface composition, and were further characterised with light scattering, electron microscopy and size exclusion chromatography (SEC). Importantly, the nanoparticles were found to be tolerable both in vitro and in vivo, without the need for any purification after particle synthesis. Pharmacokinetic and biodistribution studies

in mice, following intraperitoneal injection of the nanoparticles, revealed a long (>76 h) circulation time and accumulation in the liver.

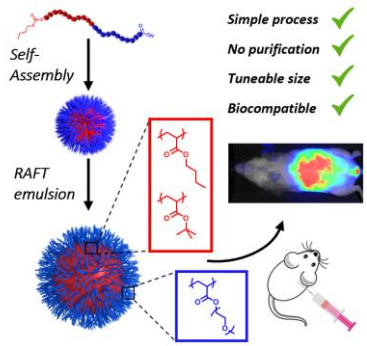

1. Introduction

Polymeric nanoparticles are well established as platforms for drug delivery and bio-imaging applications.[1, 2] Their large size promotes extended circulation times[3] and passive tumour accumulation through the enhanced permeability and retention (EPR) effect.[4, 5] Encapsulation/conjugation of chemotherapeutic agents inside these vehicles protects them from degradation by physiological processes after administration, while also facilitating their transport across the cellular membrane. Additionally, their high surface functionality can be exploited by attaching specific targeting moieties (antibodies[6], peptides[7], or glycosylated moieties[8, 9]). These properties can lead to higher therapeutic efficacy, tumour selectivity and reduced side effects for nanoparticle drug delivery vectors, in comparison to their molecular drug counterparts. [10]

In nanomedicine, and particularly for cancer therapy, polymeric nanoparticles are generally engineered to have diameters between 20 - 200 nm (to exploit the EPR effect), [4, 5, 11] a hydrophobic core for high drug loading efficiency, [12] and a cyto-compatible corona to reduce toxicity.[13] These properties can be achieved through a multitude of methods, including self-assembly of amphiphilic block-copolymers,[14, 15] or traditional emulsion polymerisation.[16] These synthetic approaches have potential disadvantages which may limit their clinical use. For instance, self-assembly of block copolymers is typically performed at low concentrations, small scales (2-5 mg mL^{-1}) and in the presence of cytotoxic organic solvents (DMF, THF or Methanol), affecting safety and synthetic reproducibility.[17] In contrast, emulsion polymerisation is highly scalable and is conventionally performed in aqueous media. However, it requires stabilisation using traditional surfactants, which can be highly cytotoxic. Furthermore, the low circulatory concentration of therapeutic nanomaterials after injection may cause the release or disassembly of amphiphilic molecules (either surfactants or block

copolymers). This can reduce the biocompatibility and increase the clearance rate of materials produced using both methods, which can have an impact in their therapeutic efficacy.[18] This can be overcome with meticulous design of covalently bound branched/brush-like polymers (unimolecular micelle)[19-21], however, achieving the large sizes (20-200 nm) and scales[17] required for these application through this method is non-trivial.

Reversible addition fragmentation chain transfer (RAFT) emulsion polymerisation provides an elegant solution to some of these problems by combining the advantages of traditional emulsion polymerisation (fast polymerisation rates, green/aqueous conditions and high scalability) with the hallmarks of controlled radical polymerisation (narrow and tuneable molecular weight distributions, block copolymer synthesis and functional end group fidelity).[22, 23] During this process, amphiphilic di-block macromolecular RAFT (macro-RAFT) agent stabilisers are assembled into micelles, with the thiocarbonylthio group within the core. These are then chain extended during the emulsion polymerisation with hydrophobic monomer (oil phase), resulting in 'frozen' uniform core-shell latex nanoparticles where the shell is comprised of the hydrophilic section of the stabilising agent. Nanoparticles prepared using this approach are adapted for biomedical applications, as the shell is covalently attached and cannot desorb from the particle during circulation. Advantageously, this process is performed in the absence of organic solvents (aqueous conditions), is highly scalable, and the stabiliser can be designed to impart biocompatibility or other additional functionality.

Nevertheless, most reports on RAFT emulsion polymerisation focus on their synthesis (kinetics and morphology),[22, 24-28] with only a few notable studies exploiting this technique to generate nanoparticles aimed at biomedical applications. For example, Stenzel and co-workers used an amphiphilic poly(glucose methacrylamide)-*b*-polystyrene macro-RAFT agent to generate

glycosylated nanoparticles, which displayed high affinity for *E. coli*.[29] Whereas, Wang and co-workers used RAFT emulsion polymerisation to control the monomer composition of the nanoparticle shell, yielding a system which release rate of a model hydrophobic drug (indomethacin) could be tuned with pH.[30] Furthermore, our group have illustrated the potential for surface modification of polyacrylamide stabilised polystyrene nanoparticles synthesised from RAFT emulsion, initially as micro-RNA carriers, and also for fluorescent labelling for studies *in vitro* and *in vivo*.[31, 32] In addition, we recently used this approach to generate well-defined mannose coated nanoparticles able to interact with lectin Concanavalin A.[33] Nonetheless, these nanoparticle systems required extensive dialysis purifications, which reduces their scalability potential. Moreover, their suitability in complex biological organisms still remains mostly unknown, with little information reported about these nanoparticles in cellular assays or live animal models.

Herein we report the synthesis of a series of core-shell polymeric nanoparticles *via* RAFT emulsion polymerisation purposely designed to impart high biocompatibility without the need of post-synthesis purification. The nanoparticles were characterised with light scattering, electron microscopy and size exclusion chromatography. Their toxicity was then evaluated *in vitro* on a colorectal carcinoma cell line (Caco-2), and *in vivo* on mouse models. Finally, a near-infrared (NIR) probe, Cyanine-7.5, was encapsulated into the nanoparticles, and preliminary pharmacokinetics and biodistribution were studied using an *in vivo* fluorescence imager.

2. Results and Discussion

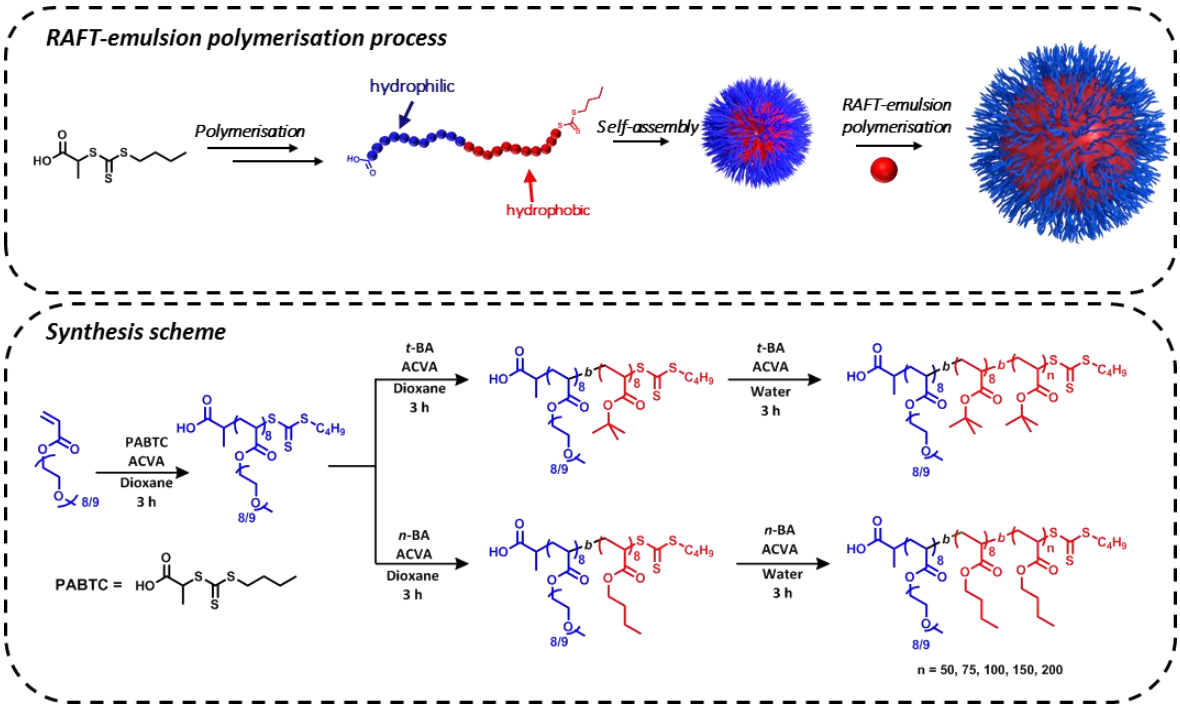

Scheme 1 Preparation of *n*-BA and *t*-BA macro-RAFT agents *via* solution RAFT polymerisation, and subsequent RAFT emulsion polymerisation to generate *n*-BA and *t*-BA nanoparticles.

2.1. Macro-RAFT agent synthesis and characterisation

Macro-RAFT agents poly[(poly(ethylene glycol methyl ether acrylate)$_8$-*block*-(*n*-butyl acrylate)$_8$] (P(PEGA)$_8$-*b*-P(*n*-BA)$_8$) and poly[(poly(ethylene glycol methyl ether acrylate)$_8$-*block*-(*t*-butyl acrylate)$_8$] (P(PEGA)$_8$-*b*-P(*t*-BA)$_8$) were synthesised in two steps (Scheme 1), using previously described conditions.[33] Initially, polymerisation of PEGA was conducted in the presence of RAFT agent PABTC, and subsequently chain extended with *tert*-butyl acrylate (*t*-BA) or *n*-butyl acrylate (*n*-BA) at 70°C. In both cases, $CHCl_3$-SEC indicated narrow molar mass distributions ($Đ$ < 1.2; Figure S1, Table S1), with shifts towards higher molecular weight after chain extension we found ^{1}H NMR spectra confirmed excellent agreement between theoretical and observed molar masses (Figure S2). Furthermore, dynamic light scattering (DLS) indicated the formation of micelles 6 nm in diameter for aqueous solutions of both P(*n*-

BA) and P(*t*-BA) macro-RAFT agents (Figure S3). ζ-potential measurements indicated negatively charged surfaces (~-10 mV), imparted by the carboxylate R group of PABTC (Table 1).

2.2. Nanoparticle synthesis *via* RAFT emulsion polymerisation

Nanoparticles of different sizes were synthesised using RAFT emulsion polymerisation according to previously described methods (Scheme 1).[33]. Briefly, the macro-RAFT agent and thermal initiator ACVA were dissolved in deionised water, sealed and purged with N_2, then deoxygenated monomer (*t*-BA for *t*-BA macro-RAFT agent, or *n*-BA for *n*-BA macro-RAFT agent) was added in batch, without feeding. Emulsions were homogenised and heated at 70°C for 3 h. Emulsion polymerisations were performed with five different DP_{target} (50, 75, 100, 150 and 200) for the third, core forming block, resulting in a library of five P(*t*-BA) and five P(*n*-BA) core-shell nanoparticles. Syntheses were performed at up to 8.4 wt% monomer at 10 mL scales (84 mg mL^{-1}), which could be easily scaled up to multi-gram reactions.[34] Full monomer conversion was attained in under 3 h, due to the well-established compartmentalisation effects found in emulsion polymerisation. This is particularly useful in a biomedical context, as residual monomer is known to be highly cytotoxic.[35] Our system can therefore be used without any further purification, as the polymerisations are performed in water. It should be noted that RAFT emulsion polymerisation procedures can be performed directly from the hydrophilic homopolymer, with the diblock formation occurring in situ. However in preliminary experiments we found this gave broad dispersity latexes and poorer molecular weight control (data not shown). SEC chromatograms of the dissolved nanoparticles indicated successful chain extension, with a significant shift from the macro-RAFT agent traces. Nonetheless, chromatograms exhibited three distinct populations: a small high molecular weight shoulder

(due to branching or bimolecular termination), a second low molecular weight population of unconsumed macro-RAFT agent, and a main narrow population of the targeted polymer (Figure 1a and 1b). As expected for controlled radical polymerisations, increasing the DP_{target} resulted in larger experimental molar masses (10,200 to 30,700 g mol^{-1} for P(*t*-BA) and 11,500 to 25,700 g mol^{-1} for P(*n*-BA)) determined by SEC. DLS traces revealed narrow monomodal size distributions (PDi ≤ 0.07; Table 1), whereby particle diameter increased from 31 to 119 nm for P(*t*-BA) and 28 to 130 nm for P(*n*-BA) nanoparticles, in accordance with DP_{target} (Figure 1c and 1d). This highlights the fine relationship between unimer molecular weight and particle size, which is a useful feature when designing nanoparticles for biomedical applications, as particle size is known to heavily influence cellular uptake and biodistribution.[36] Nanoparticle size and morphology were confirmed using Cryo-TEM, revealing spherical particles with diameters similar to those determined with light scattering (Figure 2). Furthermore, due to the carboxylic acid moiety on the surface, all nanoparticles displayed negative ξ-potential values between -35 and -50 mV, known to reduce toxicity and specific interactions.[36] Full characterisation data of the nanoparticles can be found in Table 1.

Table 1 Characterisation of the P(*n*-BA) and P(*t*-BA) nanoparticles used in this study.

Core polymer	**DP_{target}**[a]	**D_h**[b] **(nm)**	**PDi**[b]	**ζ**[c] **(mV)**	**$M_{n,th}$ (g mol^{-1})**[d]	**$M_{n,SEC}$ (g mol^{-1})**[e]	**$M_{w,SEC}$ (g mol^{-1})**[e]	**$Đ$**[e]	**M_a (Mg mol^{-1})**[f]	**N_{agg}**[g]	**$N_{agg,th}$**[h]
P(*n*-BA)	200	130	0.05	-47.3	30700	25700	48600	1.86	1060	21800	22500
	150	93	0.06	-37.8	24300	22500	34000	1.60	350	10300	10100
	100	75	0.06	-35.4	17900	18400	24400	1.39	157	6600	7400
	75	50	0.06	-37.1	14700	14200	18500	1.35	21	1200	2700
	50	28	0.06	-34.2	11500	11500	13300	1.22	6.9	520	600
P(*t*-BA)	200	119	0.05	-48.5	30700	30700	47000	1.54	777	16500	17300
	150	86	0.05	-45.1	24300	22000	34900	1.58	283	8100	8300
	100	65	0.06	-39.2	17900	16500	24400	1.47	127	5200	5100
	75	49	0.06	-42.6	14700	13300	17600	1.32	37	2100	2700
	50	31	0.07	-37.4	11500	10200	12600	1.23	13	1000	800

[a]Refers to the target DP of RAFT emulsion polymerisations performed to obtain the third core forming block. [b]Determined by DLS. [c]Determined with a Zetasizer. [d]Determined using

Equation 1 [e]Determined by $CHCl_3$-SEC (values are obtained by integrating the whole region, including all three peaks), calibrated with PMMA standards. [f] Determined by SLS. [g] Calculated using Equation S1-4.[h]Calculated using Equation 3 and 4.

To elicit if the P(PEGA) block remained at the particle surface, we used a PEG selective aggregation assay, based on the well-known property of PEG as a tannin binding agent.[37-39] This operates on a similar basis to lectin-glycopolymer assays, where addition of an agent which can bind multiple substrates (nanoparticles, polymers etc.) induces an increase in turbidity/absorbance, caused by aggregation of particles. Interestingly, a rapid increase in absorbance (at 500 nm) was observed when nanoparticles (both P(*t*-BA) and P(*n*-BA)) were treated with tannic acid (Figure S4), suggesting high availability of PEG in their surface. Unfortunately, this cannot be used to quantify how many chains are available at the corona. This was further studied using static light scattering (SLS), which allows to determine the weight average molar mass of a whole nanoparticle, and therefore, the number of polymer building blocks per particle (N_{agg}). Scattering profiles of all ten nanoparticle suspensions (at four different concentrations) were acquired across 8 angles (Figure S5). Larger apparent particle molar masses (M_a) were observed with increasing nanoparticle diameter for both P(*t*-BA) and P(*n*-BA) nanoparticles. By dividing the M_a values obtained by the M_w of their respective unimers (obtained previously from SEC), we could approximate the number of unimers per particle (N_{agg}). Surprisingly, N_{agg} increased dramatically with larger particle sizes, ranging from < 1000 for the smallest nanoparticles, up to > 15,000 for the largest (Table 1), and show excellent agreement with theoretical N_{agg} values (Equation 3 and 4; Table 1). This trend observed can be rationalised as larger nanoparticles have more surface area, hence require greater stabilisation than smaller nanoparticles. Moreover, our results suggests that some level of rearrangement of the macro-RAFT agents occurs during the RAFT emulsion polymerisation process, leading to different N_{agg} depending on particle size. [40]

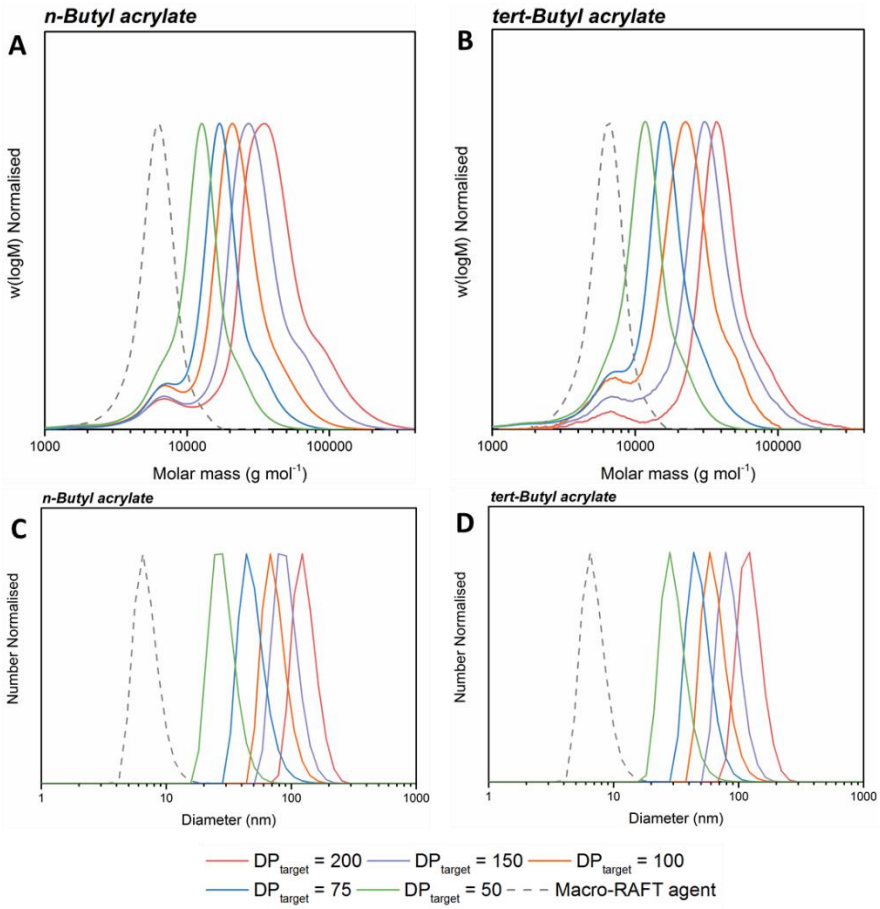

Figure 1. $CHCl_3$-SEC chromatograms depicting the increasing DP_{target} chain extensions of (A) $P(PEGA)_8$-*b*-$P(n\text{-}BA)_8$ with *n*-butyl acrylate and (B) $P(PEGA)_8$-*b*-$P(t\text{-}BA)_8$ with *t*-butyl acrylate. Chromatograms obtained by dissolving dried nanoparticles in SEC eluent. DLS traces (number distribution) of all (C) poly(*n*-butyl acrylate) and (D) poly(*tert*-butyl acrylate) nanoparticles and their respective macro-RAFT agents (dashed grey lines) sizes at 25˚C diluted 1/1000 in pure water.

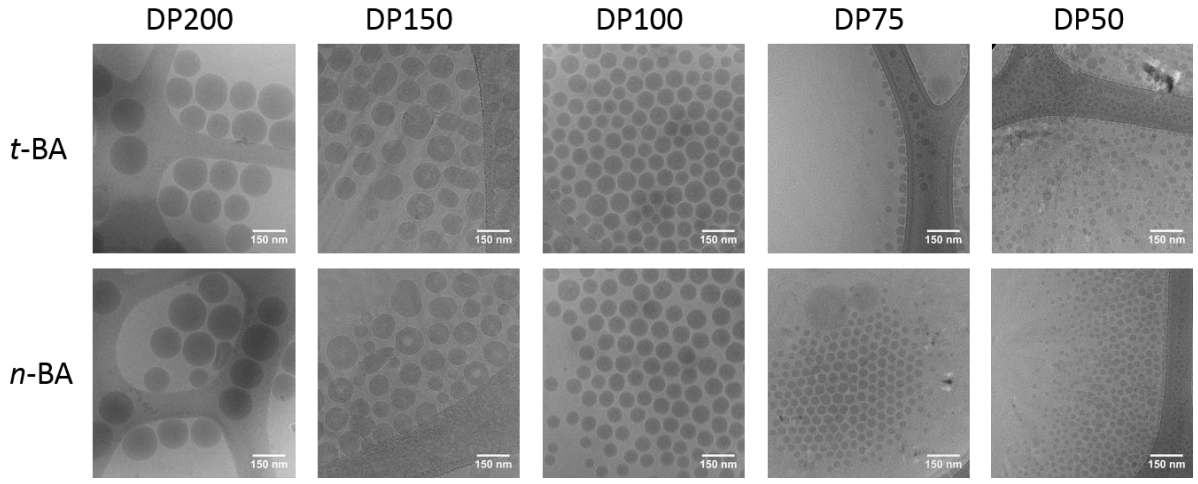

Figure 2. Cryo-TEM images of undiluted P(*t*-BA) (top row) and P(*n*-BA) (bottom row) nanoparticles deposited on lacey carbon coated grids.

2.3. *In vitro* and *in vivo* biocompatibility

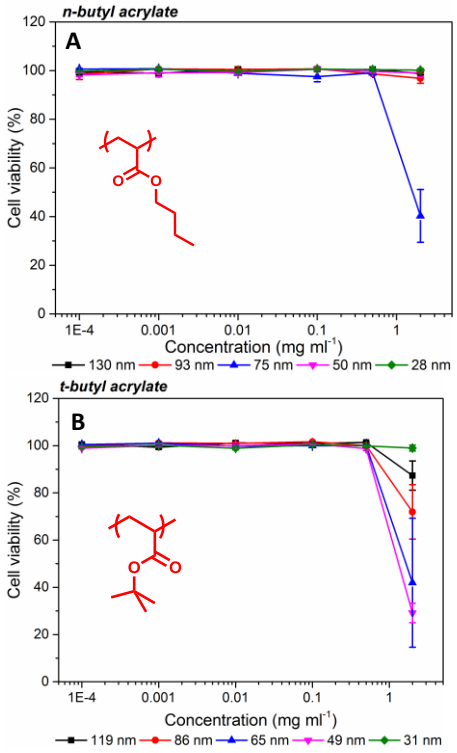

Figure 3. Antiproliferative activity of P(*n*-BA) (28 – 130 nm) and P(*t*-BA) (31 – 119 nm) on Caco-2 cells over 72 h at 2, 0.5, 0.2, 0.01, 0.001 and 0.0001 mg mL^{-1} assessed using the sulforhodamine B assay. Data is expressed as the arithmetic mean ± standard deviation of two independent experiments performed in triplicate (N=6).

The biocompatibility of all ten nanoparticles was determined both *in vitro* and *in vivo* without prior purification. Initially, cells from a human colorectal adenocarcinoma cell line (Caco-2) were exposed to different concentrations of nanoparticles (2 $mg.mL^{-1}$ – 100 $ng.mL^{-1}$) for 72 h, and cell viability was measured using the sulforhodamine B (SRB) assay. None of the nanoparticles inhibited cell growth up to 0.5 mg mL^{-1}. Nonetheless, the 75 nm P(*n*-BA), and all P(*t*-BA) nanoparticles with D_h > 31 nm reduced cell proliferation at 2 mg mL^{-1} (Figure 3). However, this concentration is far beyond any envisaged clinical dosage for these, or other similar systems.

It has previously been shown that there is little particle size dependency on *in vivo* biodistribution and toxicity,[41] therefore the 49 and 86 nm P(*t*-BA) and, 50 and 93 nm P(*n*-BA) nanoparticles were selected as representative treatments for *in vivo* toxicity experiments. In a first experiment, wild type ICR CD1 mice were treated with a single dose (1.2 mg kg^{-1} and 12 mg kg^{-1}) or 7-day daily repeated (subchronic; injections performed for 5 days and weight monitored for 7 total) intraperitoneal (i.p.) injection of nanoparticles (only at the higher concentration) or vehicle control. Body weight, appearance of coat and clinical behaviour were monitored daily for a period of 7 days after administration (Figure 4). No clinical toxicity was apparent for any of the nanoparticles tested, both after acute or subchronic dosing. No statistically significant differences in body weight changes were found between nanoparticles- and vehicle-treated mice over the 7-day span (p = 0.15 for single injection and p = 0.15 for subchronic dosing). Importantly none of the individual mice showed any reduction in body weight or any "clinical" toxicity signs over the seven day period.

The excellent tolerability observed both *in vitro* and indeed *in vivo* is likely due to the P(PEGA) shell present on all the nanoparticles, which is known to reduce the immune response and other unwanted interactions within the organism.[42] This is in accordance with a report from Tamanoi and co-workers, showing limited toxicity for intraperitoneally administered mesoporous silica nanoparticles through a full serological, haematological and histopathological investigation.[43]

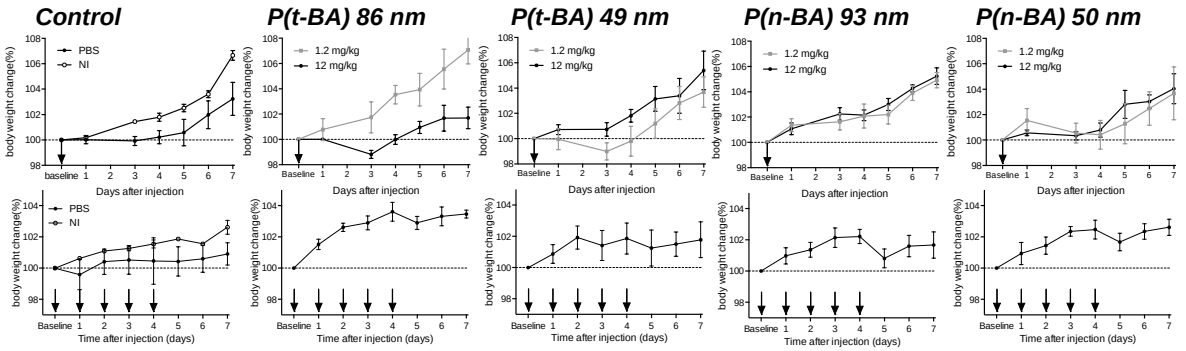

Figure 4. Acute (top row) and 7-day repeated (bottom row) toxicity in mice for the 50 and 93 nm *n*-BA, and 49 and 86 nm *t*-BA nanoparticles at both 1.2 mg kg^{-1} (red lines) and 12 mg kg^{-1} (blue lines), measured as a function of animal body weight monitored over 7 days (N=3 for acute toxicity, N=6 for 7-day repeated dosing). Controls of PBS injection (green lines; N=3 for both acute toxicity and 7-day dosing) and non-injected (purple lines; N=2 for both acute toxicity and 7-day dosing) mice are also displayed. Data is reported as mean ± SEM. Arrows indicate administration points.

2.4. Fluorescent labelling and *in vivo* biodistribution

NIR fluorescence is a highly sensitive and non-invasive method to study pharmacokinetics, biodistribution and organ accumulation.[44] As a model study, we labelled the 50 nm P(*n*-BA) nanoparticles with NIR dye Cyanine 7.5 amine (Cy7.5), following an adapted procedure from Resch-Genger and co-workers.[45] This approach works by swelling the particles with *ca.* 10% organic solvent, in the presence of the hydrophobic dye, partitioning it into the core of the nanoparticles. The particles were then purified by extensive dialysis and analysed with fluorescence spectroscopy to confirm dye internalisation (Figure S6).

A dilute suspension of NIR-particles (1.2 mg kg^{-1}) was administered (i.p.) to adult male CD1 mice, and the nanoparticle distribution was followed over 76 h using a LICOR Pearl® Trilogy *in vivo* fluorescence imager. Prior to injection, no fluorescence was observed from any part of the animal (Figure 5a). In contrast, a bright signal from the abdominal cavity was detected immediately after i.p. injection, which decreased rapidly within 2 h, thus likely reflecting uptake and distribution into the systemic circulation (Figure 5a and 5b, Figure S7). This was

followed by slow clearance, over the next 74 h (Figure 5a and 5b), with 36% of the injected dose being retained within the animal at the end of the experiment (76 h; Figure S7). *Ex vivo* imaging of the excised organs at 76 h after injection revealed high nanoparticle accumulation in the liver. Negligible amounts were found in the heart or white adipose tissue of the animal, while small but significant quantities were observed in the intestine, spleen and kidneys (Figure 5c and S8). However, some of this signal might be due to direct particle adsorption to the peritoneal organs after i.p. injection, however some subsequent release into systemic will still occur. Additionally, the intestinal signal could be partly attributed to the presence of chlorophyll in the animal diet, resulting in faecal NIR fluorescence in non-injected mice (Figure S9).[46] It is unlikely, however, that diet is solely responsible for the detected intestinal fluorescence. A new NIR signal appears around the anus area 1 h after administration, which is not observable in untreated animals. Therefore, a significant proportion of the intestinal emission should be associated with the nanoparticles. This might suggest that our particles could be excreted *via* the gastrointestinal/ hepatobiliary system, a well-known elimination route for nanoparticles, as their size is above the renal filtration threshold of 4.5-5 nm.[47, 48]

There are relatively few reports on the biodistribution and pharmacokinetics of intraperitoneally administered polymeric nanoparticles.[49, 50] Nonetheless the described nanoparticles can still be compared to similar studies using non-polymeric nanomaterials. For example, in contrast to 100 nm mesoporous silica nanoparticles (MSN), our system show far quicker clearance from the peritoneal cavity, (64% after 76 h compared to 0-5% after 160 h), but greater accumulation in the abdominal organs (liver, spleen, intestine).[43] Meanwhile, a similar study on gold nanoparticles revealed almost complete clearance within 24 h, with similar accumulation in in the liver and spleen.[51]

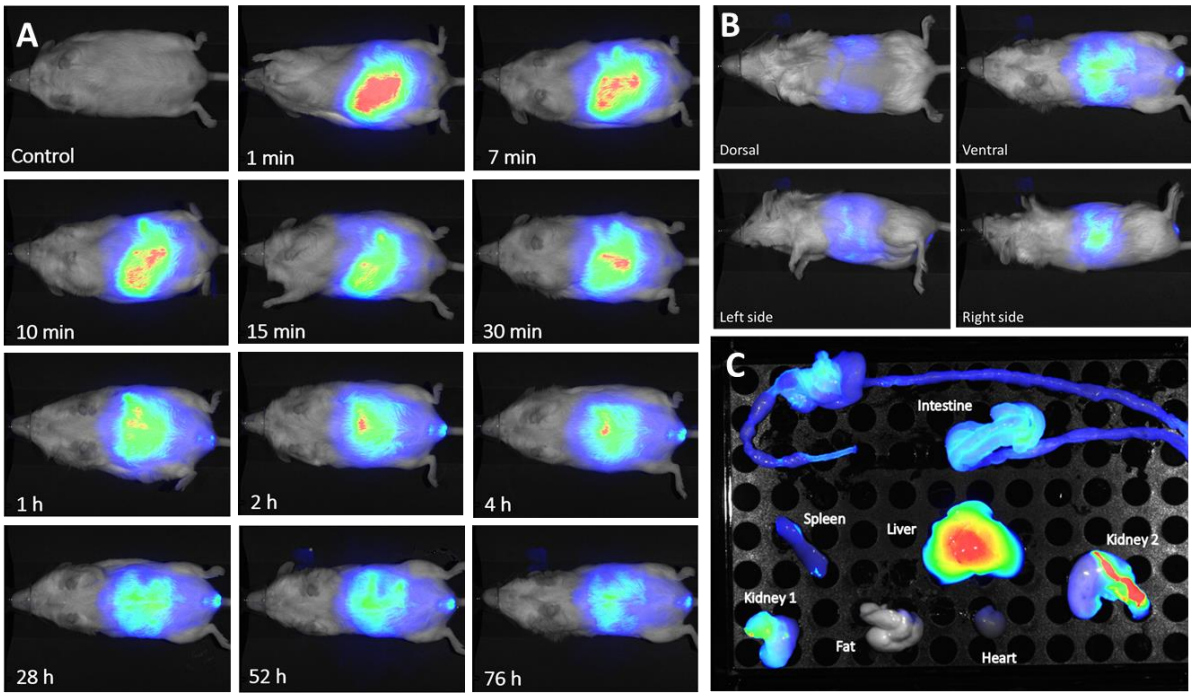

Figure 5. Biodistribution in male CD1 mouse after a single i.p. injection of Cy7.5 loaded 50 nm P(*n*-BA) nanoparticles (1.2 mg/kg). Distribution was monitored using the 800 nm fluorescence channel of a LICOR Pearl® Trilogy. (A) Pharmacokinetic study over 76 h (B) Ventral, dorsal and lateral views of a mouse 76 h after injection (C) *Ex vivo* images of organs samples 76 h after injection.

3. Conclusions

By generating a library of P(PEGA) shell and P(*n*-BA) and P(*t*-BA) core nanoparticles, we have shown that RAFT emulsion polymerisation is a highly versatile method to synthesise biocompatible nanomaterials. Furthermore, this approach is particularly interesting for its industrial scale up potential as reactions are performed in environmentally friendly aqueous environments, and reach full consumption of cytotoxic monomer within a matter of hours. These advantages allow use of the nanoparticles for biological purposes without prior purification. The particles displayed no toxicity in our *in vitro* and *in vivo* experiments, and relatively long retention in mice post administration with high accumulation in the liver. Overall, our synthetic approach has the potential to influence future nanoparticle design aimed at biomedical applications.

4. Experimental

4.1 Materials

Poly(ethylene glycol) methyl ether acrylate (PEGA, average M_n = 480 g mol^{-1}), *n*-butyl acrylate (*n*-BA, >99%) and *t*-butyl acrylate (t-BA 98%), Bromo-propionic acid (>99%), 1-butanethiol (99%), carbon disulphide (>99%) and tannic acid (ACS reagent) were obtained from Sigma-Aldrich. All monomers above were passed through basic aluminium oxide to remove inhibitor before use. Chloroform-d_3 (99.8% D atom), was obtained from Sigma Aldrich and used for ^{1}H NMR spectroscopy. Thermal initiator 4,4′-azobis(4-cyanovaleric acid) (ACVA, >98%, Aldrich), was used as received. Cyanine 7.5 amine was purchased from Lumiprobe. TEM grids were purchased from EM Resolutions Ltd (Sheffield, UK). RAFT agent, 2-(((butylthio)carbonothioyl)thio)propanoic acid (PABTC) was synthesised as previously described.[22]

4.2 Characterisation methods

4.2.1. ^{1}H NMR spectroscopy

^{1}H NMR spectra were recorded on a Bruker DPX-250, DPX-300 or DPX-400 spectrometer using deuterated solvent (materials section).

4.2.2. Size exclusion chromatography

SEC was performed using an Agilent 390-LC MDS instrument equipped with differential refractive index (DRI), viscometry (VS), dual angle light scatter (LS) and two wavelength UV detectors. The system was equipped with 2 x PLgel Mixed C columns (300 x 7.5 mm) and a PLgel 5 µm guard column. The eluent was $CHCl_3$ with 2 % TEA (triethylamine) additive.

Samples were run at 1 ml/min at 30'C. Poly(methyl methacrylate), and polystyrene standards (Agilent EasyVials) were used for calibration. Ethanol was added as a flow rate marker. Analyte samples were filtered through a GVHP membrane with 0.22 μm pore size before injection. Respectively, experimental molar mass ($M_{n,SEC}$) and dispersity ($Đ$) values of synthesized polymers were determined by conventional calibration using Agilent GPC/SEC software.

$$M_{n,th} = \frac{[M]_0 \, pM_M}{[CTA]_0} + M_{CTA}$$

Equation 1. Calculation of theoretical number average molar mass ($M_{n,th}$) where $[M]_0$ and $[CTA]_0$ are the initial concentrations (mol dm^{-3}) of monomer and chain transfer agent respectively. p is the monomer conversion as determined by ^1H NMR spectroscopy. M_M and M_{CTA} are the molar masses (g mol^{-1}) of the monomer and chain transfer agent respectively.

4.2.3. Dynamic light scattering, size and zeta-potential

Size and ζ-potential measurements were carried out using a Malvern Zetasizer Nano-ZS at 25°C with a 4 mW He-Ne 633 nm laser at a scattering angle of 173° (back scattering). Measurements were taken assuming the refractive index of: polyethylene glycol for diblock macro-RAFT agents, and the refractive index of the core material (e.g n-butyl acrylate or t-butyl acrylate) for latex particles. DLS samples of latex particles were prepared by diluting by 1000 with 1 mL of water and measured unfiltered in 1.5 mL polystyrene cuvettes for measuring size and a Malvern DTS-1070 zeta cuvette for ζ-potential. Diblock copolymer macro-RAFT agent samples were measured at the concentration of a typical RAFT emulsion polymerization (15 mg mL^{-1}). Samples were incubated for 60 seconds at 25°C prior to measurement. Measurements were repeated three times with automatic attenuation selection and measurement position. Results were analysed using Malvern DTS 6.20

software. PDi values were calculated using the following equation. Measurements of ζ-potential were modelled with the Smoluchowski theory.

$$PDi = \frac{\sigma^2}{d_h^2}$$

Equation 2. Calculation of nanoparticle polydispersity (PDi) from standard deviation (σ), and diameter (d)

4.2.4. Static light scattering

Static light scattering measurements were performed with an ALV-CGS3 system (ALV-Langen) operating with a vertically polarized laser with wavelength λ = 632.8 nm. Measurements were conducted at 20°C over a range of angles (20, 30, 50, 70, 90, 110, 130 and 150 degrees) and concentrations in aqueous conditions. Samples were measured unfiltered. The intercepts for each concentration of plots for q vs KC/R were then plotted against concentration, and the intercept of the latter graph was taken as the apparent molar mass. Full details can be found in the supplementary information (Equation S1-S5).

4.2.5. Calculation of the theoretical number of aggregation

The theoretical number of aggregation was determined, first by evaluating the number of particles per unit volume (N_p; Equation 3), and then dividing the number of macro-RAFT agents per unit volume by this value (Equation 4).

$$N_p = \frac{6\tau}{\pi(D_h)^3 d_p}$$

Equation 3. Determination of the number of particles per volume. N_p = number of particles per mL τ = solids content (g mL^{-1}), D_h = average hydrodynamic particle diameter, d_p = density of polymeric core.

$$N_{agg} = \frac{[macro-RAFT]\cdot N_A}{N_p}$$

Equation 4. Number of macro-RAFT agents per particle (N_{agg}).

4.2.6. Different Refractometry

Measurements were performed with an RI-101 from Shodex (λ_0=632 nm). The refractive index increment was measured in water using 5 concentrations of nanoparticles and the dn/dC was calculated by equation S6.

4.2.7. Cryogenic-transmission electron microscopy

8 µL of the sample was applied to a glow-discharged lacey carbon grid (EM Resolutions), blotted for 4 seconds and frozen in liquid propane/ethane (30%/70% v/v) using a custom-made plunge-freezing device. Grids were imaged in the JEOL 2200FS with a Gatan K2 camera and a Gatan 914 cryo-holder cooled to -180 ˚C.

4.2.8. Fluorescence spectroscopy

Fluorescence emission spectra were measured using an Agilent Cary Eclipse fluorescence spectrometer. Studies were performed by exciting at the absorption maxima of Cy7.5 (780 nm) and measured from 785 nm to 900 nm. The photomultiplier voltage was set such that the maxima was below 1000 arbitrary units. Samples were diluted 1: 100 fold in pure water for measurement.

4.3. Synthetic Procedures

4.3.1 $P(PEGA)_8$ synthesis

Procedures adapted from literature conditions.[33] PABTC (0.31 g, 1.30 x 10^{-3} mol), PEGA (5 g, 10.4 x 10^{-3} mol) and ACVA (from a pre-made stock solution in 1,4-dioxane) (18 mg, 6.51 x 10^{-5} mol) were dissolved in 4.9 mL 1,4-dioxane in a 25 mL round bottom flask equipped with a magnetic stirrer bar. The solution was fitted with an appropriate sized rubber septum, and purged with nitrogen for 20 minutes. The round bottom flask was subsequently immersed in an oil bath preheated to 70°C and stirred for 3 h. The reaction vessel was cooled to ambient temperature and opened to oxygen to quench further polymerisation. The polymer was purified by precipitation into a mixture of 20% hexane and 80% diethyl ether (v/v), collected, and the precipitation repeated once more. Finally, the precipitated polymer was dissolved in DCM, transferred to a 20 mL vial, the DCM evaporated and dried in a vacuum oven overnight at 40°C to yield $P(PEGA)_8$ as a yellow viscous liquid (4.5 g).

4.3.2. Macro-RAFT agent synthesis

All diblock copolymer macro-RAFT agents were synthesized with the following general procedure, as an example $P(PEGA)_8$-P(*n*-$BA)_8$ is described.[33] Full details can be found in table S1. *n*-Butyl acrylate (0.25 g, 1.95 x 10^{-3} mol) and 0.68 mL of a 5 mg ml^{-1} ACVA stock solution

in 1,4-dioxane (3.4 mg, 1.21 x 10^{-5} mol) were added to P(PEGA)$_8$ (0.94 g, 2.43 x 10^{-4}). The polymerisation mixture was purged with nitrogen for 20 minutes and heated to 70°C for 3 h. The resulting polymer solution was cooled to room temperature and subsequently purified by precipitation in hexane. The yellow viscous liquid was re-dissolved in dichloromethane and the precipitation was repeated once more. Finally, the solvent was evaporated under reduced pressure to yield the di-block macro-RAFT agent as a yellow viscous liquid (0.95 g).

4.3.3. RAFT emulsion polymerisation procedure

Nanoparticles of different sizes and core compositions were prepared using previously described conditions, full details can be found in Table S2.[33] As an example synthesis of P(PEGA)$_8$-*b*-P(*t*-BA)$_8$-*b*-P(*t*-BA)$_{200}$ is described. 1.43 mL of a 10 mg mL^{-1} sodium hydroxide stock solution (14.3 mg, 3.6 x 10^{-4} mol) was added to a suspension of ACVA (50 mg, 1.8 x 10^{-4} mol) in water (8.57 mL) and stirred for 30 min to ensure full solubility. P(PEGA)$_8$-*b*-P(*t*-BA)$_8$ (0.145 g, 2.85 x 10^{-5} mol) was dissolved in 7.71 mL of water, in a 25 mL round bottomed flask and equipped with a magnetic stirrer. 1.45 mL of the above ACVA stock solution was added, the vial fitted with a rubber septum, and the solution was deoxygenated with dinitrogen gas for 20 minutes. Deoxygenated *t*-BA (0.83 mL, 2.14 x10^{-3} mol) was added *via* syringe and the polymerisation mixture was immersed in a 70°C oil bath and stirred for 3 h at 400 RPM. Monomer conversion was determined *via* gravimetric techniques.

4.3.4. PEG binding assay

Tannic acid was diluted to a concentration of 10 µg mL^{-1} in deionised water. Nanoparticle suspensions were diluted with deionised water to a concentration of 10 µg mL^{-1}. 1 mL of the nanoparticle suspensions were transferred to a polystyrene cuvette and placed in the UV-VIS spectrometer. Absorbance measurements were recorded once every 1 s at 500 nm. After 1 min,

250 µL of the tannic acid solution was added *via* micropipette and mixed briefly without allowing the pipette tip into the detection window. The absorption was monitored for a further 4 minutes.

4.3.5. Encapsulation of Cyanine 7.5

Cy7.5 (1 mg) was added to 1 mL of 10% DMF in THF and sonicated until the powder had fully dissolved. 100 µL of the Cy7.5 solution was added to 900 µL of nanoparticle suspension and shaken for 1 h. The suspension was then dialysed (3500-5000 Da MWCO) against pure water for 48 h to remove residual DMF and THF. Loaded particles were used immediately after encapsulation for *in vivo* fluorescence studies.

4.4. In vitro studies

4.4.1. Cell culture

Caco-2 cells were purchased from ECACC (European Collection of Animal Cell Culture, Salisbury, UK; ECACC 86010202) and cultured as monolayers at 37˚C in a humidified atmosphere containing 5% CO_2. Cells were cultured in a 50:50 mixture of Dulbecco's Modified Eagle Medium (DMEM) and HAMS F12 supplemented with 10% of foetal calf serum, 1 % of L-glutamine and 1% penicillin/streptomycin. Cells were sub-cultured at regular intervals and passages made by trypsinising cells when at 80-90% confluence.

4.4.2. Cell viability assay

Caco-2 cells were seeded at a density of 10,000 cells per well in a flat bottomed clear 96 well plate and incubated for 24 h. Nanoparticles were diluted with cell culture medium into a 2 mg ml^{-1} suspension. The stock solution was then serially diluted to make solutions of 100 ng ml^{-1}, 1 µg ml^{-1}, 10 µg ml^{-1}, 100 µg ml^{-1}, 500 µg ml^{-1} and 2 mg mL^{-1}. The cells were incubated in the

presence of the nanoparticle suspensions for 72 h. The sulforhodamine B assay was used to determine cell viability as a function of biomass fixed on the well plate surface, relative to untreated controls. In short, 50 µL of cold 50% trifluoroacetic acid were added to each well of the plate and left to incubate for 1 h at 4°C, the plate was subsequently washed 10 times with slow running tap water to remove excess trifluoroacetic acid. Then, the plate was heated gently with warm air to remove moisture, and 50 µL of 0.4% sulforhodamine B (prepared in 1% acetic acid) were added to each well and incubated at ambient temperature for 30 min. Excess dye was removed by washing the plate 5 times with 1% acetic acid. Finally, 200 µL of 10 mM Tris base solution (pH 10.5) were added to each well and incubated at ambient temperature for 1 h before absorbance of each well was measured at 570 nm on a BioRad iMark 96-well microplate reader. All experiments were carried out as duplicates of triplicates in two independent experiments (N=6).

4.5. In vivo studies

4.5.1. Animal handling

All *in vivo* studies were conducted on adult male CD1 mice purchased from Charles River (UK). Upon arrival, mice were allowed to adjust to the new environmental condition for at least two weeks. Humidity and temperature were kept between 45 to 60% and between 20 to 24°C, respectively, and animals had 12 hours of light per with light onset at 07:00. Mice had ad libitum access to food and water. All in vivo experiments were carried out in accordance with the Animal Scientific Procedure Act 1986 under the Procedure Project Licence (PPL) number 70/3685.

4.5.2. In vivo toxicity studies

For acute, single dose toxicity evaluation, 29 six to seven week old male mice were randomised into eight groups and intraperitoneally (i.p.) injected with the different nanoparticles (N=3/group), vehicle (PBS, N=3) or nothing (N=2). Nanoparticle groups were injected with 49 and 86 nm P(*t*-BA), and 50 and 93 nm P(*n*-BA) nanoparticles at either 1.2 mg kg^{-1} (0.2 mg ml^{-1} in 200 µl PBS) or 12 mg kg^{-1} (2 mg ml^{-1} in 200 µl PBS). Of note, nanoparticle dilutions were prepared in sterile PBS under aseptic conditions and stored at 2 to 8°C until treatment. After injection, mice were monitored daily for the following 7 days and body weight as well as signs of pain or distress were recorded.

For the repeat dosing study, 35 six to seven weeks old male mice were randomised into four nanoparticle treatment groups (N=6/groups) and 2 control groups (PBS N=3; no-injection N=2) as described above. Each mouse was i.p. injected daily with 12 mg kg^{-1} (200 µl of 2 mg ml^{-1}) of one of 4 types of nanoparticles, i.e. 49 or 86 nm of P(*t*-BA) or, 50 or 93 nm of P(*n*-BA), or PBS for five consecutive days. The second control group received no injection. After the first injection, mice were monitored daily for the following 8 days and body weight as well as signs of pain or distress were recorded. Data was analysed with a two-way ANOVA with repeated measures.

4.5.3. In vivo biodistribution

For biodistribution studies, mice were injected intraperitoneally with a single dose of Cy 7.5 labelled P(*n*-BA) 50 nm nanoparticles (1.2 mg kg^{-1}). Fluorescence was recorded using a LICOR Pearl® Trilogy *in vivo* imager in the 800 nm channel in intervals for up to 76 h post injection. Kinetic *in vivo* fluorescence profiles were obtained by quantifying the total fluorescence of one region of interest encompassing the whole animal using open access

software Image Studio Lite™. Organs were excised and imaged immediately after euthanasia with anaesthetic overdose. Organ fluorescence/unit area was established by drawing around each organ and dividing this value by the area reported in the software.

Supporting Information

Supporting Information is available from the Wiley Online Library

Acknowledgements

We thank CRUK/EPSRC (C53561/A19933; PG; CSC; KA; HXM; FL; SP), the German Research Foundation (DFG, GZ; HA 7725/1-1; MH) the Warwick Impact Fund (RD) and the Royal Society Wolfson Merit Award (WM130055; SP) for financial support. We are grateful to LICOR inc. for access to a Pearl® Trilogy imaging system for *in vivo* experiments. The staff of the BSU at Warwick are thanked for animal husbandry.

Received: Month XX, XXXX; Revised: Month XX, XXXX; Published online:
((For PPP, use "Accepted: Month XX, XXXX" instead of "Published online")); DOI: 10.1002/marc.((insert number)) ((or ppap., mabi., macp., mame., mren., mats.))

Keywords: biocompatible nanoparticle, RAFT emulsion polymerisation, core-shell, tuneable nanoparticle.

References

[1] M. Elsabahy, K. L. Wooley, *Chem. Soc. Rev.* **2012**, *41*, 2545.

[2] M. Beija, R. Salvayre, N. Lauth-de Viguerie, J.-D. Marty, *Trends Biotechnol.* **2012**, *30*, 485.

[3] F. Alexis, E. Pridgen, L. K. Molnar, O. C. Farokhzad, *Mol. Pharm.* **2008**, *5*, 505.

[4] H. Maeda, *J. Control. Release* **2012**, *164*, 138.

[5] J. Fang, H. Nakamura, H. Maeda, *Adv. Drug Delivery Rev.* **2011**, *63*, 136.

[6] D. A. Richards, A. Maruani, V. Chudasama, *Chemical Science* **2016**, *8*, 63.

[7] M. Roveri, M. Bernasconi, J.-C. Leroux, P. Luciani, *J. Mat. Chem. B* **2017**, *5*, 4348.

[8] B. Kang, T. Opatz, K. Landfester, F. R. Wurm, *Chem. Soc. Rev.* **2015**, *44*, 8301.

[9] M. Pröhl, S. Seupel, P. Sungur, S. Höppener, M. Gottschaldt, J. C. Brendel, U. S. Schubert, *Polymer* **2017**, *133*.

[10] L. Zhang, F. Gu, J. Chan, A. Wang, R. Langer, O. Farokhzad, *Clin. Pharmacol. Ther.* **2008**, *83*, 761.

[11] H. Maeda, J. Wu, T. Sawa, Y. Matsumura, K. Hori, *J. Control. Release* **2000**, *65*, 271.

[12] X. Tao, S. Jin, D. Wu, K. Ling, L. Yuan, P. Lin, Y. Xie, X. Yang, *Nanomaterials* **2015**, *6*, 2.

[13] A. Verma, F. Stellacci, *Small* **2010**, *6*, 12.

[14] A. Rösler, G. Vandermeulen, H.-A. Klok, *Adv. Drug Delivery Rev.* **2001**, *53*, 95.

[15] J. Zhang, J. Tanaka, P. Gurnani, P. Wilson, M. Hartlieb, S. Perrier, *Polym. Chem.* **2017**, *8*, 4079.

[16] R. G. Gilbert, G. T. Russell, "*Emulsion polymerization : a mechanistic approach*", London : Academic press, 1995.

[17] R. Paliwal, J. R. Babu, S. Palakurthi, *AAPS PharmSciTech* **2014**, *15*, 1527.

[18] T. Sun, Y. S. Zhang, B. Pang, D. C. Hyun, M. Yang, Y. Xia, *Angew. Chem., Int. Ed.* **2014**, *53*, 12320.

[19] G. Cheng, A. Böker, M. Zhang, G. Krausch, A. H. E. Müller, *Macromolecules* **2001**, *34*, 6883.

[20] M. Hartlieb, T. Floyd, A. B. Cook, C. Sanchez-Cano, S. Catrouillet, J. A. Burns, S. Perrier, *Polym. Chem.* **2017**, *8*, 2041.

[21] J. Tanaka, S. Tani, R. Peltier, E. H. Pilkington, A. Kerr, T. P. Davis, P. Wilson, *Polym. Chem.* **2018**.

[22] C. J. Ferguson, R. J. Hughes, D. Nguyen, B. T. Pham, R. G. Gilbert, A. K. Serelis, C. H. Such, B. S. Hawkett, *Macromolecules* **2005**, *38*, 2191.

[23] P. B. Zetterlund, S. C. Thickett, S. Perrier, E. Bourgeat-Lami, M. Lansalot, *Chem. Rev.* **2015**, *115*, 9745.

[24] M. Chenal, L. Bouteiller, J. Rieger, *Polym. Chem.* **2013**, *4*, 752.

[25] N. P. Truong, M. V. Dussert, M. R. Whittaker, J. F. Quinn, T. P. Davis, *Polym. Chem.* **2015**, *6*, 3865.

[26] W. Zhang, F. D'Agosto, O. Boyron, J. Rieger, B. Charleux, *Macromolecules* **2012**, *45*, 4075.

[27] D. E. Ganeva, E. Sprong, H. de Bruyn, G. G. Warr, C. H. Such, B. S. Hawkett, *Macromolecules* **2007**, *40*, 6181.

[28] I. Chaduc, A. Crepet, O. Boyron, B. Charleux, F. D'Agosto, M. Lansalot, *Macromolecules* **2013**, *46*, 6013.

[29] S. R. S. Ting, E. H. Min, P. B. Zetterlund, M. H. Stenzel, *Macromolecules* **2010**, *43*, 5211.

[30] G. Jiang, Y. Wang, R. Zhang, R. Wang, X. Wang, M. Zhang, X. Sun, S. Bao, T. Wang, S. Wang, *ACS Macro Lett.* **2012**, *1*, 489.

[31] C. K. Poon, O. Tang, X.-M. Chen, B. T. T. Pham, G. Gody, C. A. Pollock, B. S. Hawkett, S. Perrier, *Biomacromolecules* **2016**, *17*, 965.

[32] C. K. Poon, O. Tang, X.-M. M. Chen, B. Kim, M. Hartlieb, C. A. Pollock, B. S. Hawkett, S. Perrier, *Macromol. Biosci.* **2016**.

[33] P. Gurnani, A. M. Lunn, S. Perrier, *Polymer* **2016**, *106*, 229.

[34] N. P. Truong, J. F. Quinn, A. Anastasaki, M. Rolland, M. N. Vu, D. M. Haddleton, M. R. Whittaker, T. P. Davis, *Polym. Chem.* **2017**, *8*, 1353.

[35] S. S. Gosavi, S. Y. Gosavi, R. K. Alla, *Dent. Res. J.* **2010**, *7*, 82.

[36] C. He, Y. Hu, L. Yin, C. Tang, C. Yin, *Biomaterials* **2010**, *31*, 3657.

[37] H. P. S. Makkar, M. Blümmel, K. Becker, *Br. J. Nutr.* **1995**, *73*, 897.

[38] J. Niu, D. J. Lunn, A. Pusuluri, J. I. Yoo, M. A. O'Malley, S. Mitragotri, T. H. Soh, C. J. Hawker, *Nat. Chem.* **2017**, *9*.

[39] N. Silanikove, N. Gilboa, I. Nir, A. Perevolotsky, Z. Nitsan, *J. Agric. Food Chem.* **1996**, *44*, 199.

[40] D. E. Ganeva, E. Sprong, H. de Bruyn, G. G. Warr, C. H. Such, B. S. Hawkett, *Macromolecules* **2007**, *40*, 6181.

[41] S. Hirn, M. Semmler-Behnke, C. Schleh, A. Wenk, J. Lipka, M. Schäffler, S. Takenaka, W. Möller, G. Schmid, U. Simon and W. G. Kreyling, *Eur. J. Pharm. Biopharm.*, 2011, 77, 407-416.

[42] J. V. Jokerst, T. Lobovkina, R. N. Zare, S. S. Gambhir, *Nanomedicine* **2011**, *6*, 715.

[43] J. Lu, M. Liong, Z. Li, J. I. Zink, F. Tamanoi, *Small* **2010**, *6*, 1794.

[44] J. Eichler, J. Knof, H. Lenz, *Radiat. Environ. Biophys.* **1977**, *14*, 239.

[45] T. Behnke, C. Würth, K. Hoffmann, M. Hübner, U. Panne, U. Resch-Genger, *J. Fluoresc.* **2011**, *21*, 937.

[46] L. Fan, Q. Wu, M. Chu, *Int. J. Nanomedicine* **2012**, *7*, 3071.

[47] H. Choi, W. Liu, P. Misra, E. Tanaka, J. P. Zimmer, B. Ipe, M. G. Bawendi, J. V. Frangioni, *Nat. Biotech.* **2007**, *25*, 1165.

[48] M. Longmire, P. L. Choyke, H. Kobayashi, *Nanomedicine* **2008**, *3*, 703

[49] L. H. Reddy, R. S. R. Murthy, *Biomed. Pap.* **2004**, *148*, 161.

[50] P. Maincent, P. Thouvenot, C. Amicabile, M. Hoffman, J. Kreuter, P. Couvreur, J. P. Devissaguet, *Pharm. Res.* **1992**, *9*, 1534.

[51] R. R. Arvizo, O. R. Miranda, D. F. Moyano, C. A. Walden, K. Giri, R. Bhattacharya, D. J. Robertson, V. M. Rotello, J. M. Reid, P. Mukherjee, *PLoS One* **2011**, *6*.

RAFT emulsion polymerization to produce biocompatible PEGylated nanoparticles is reported. This synthesis approach allows for different core composition and particle sizes to be synthesized. The nanoparticles were highly tolerated *in vitro* and *in vivo*, with no inherent toxicity observed after multiple injections, and biodistribution studies showing high nanoparticle accumulation in the liver.

P. Gurnani, C. Sanchez-Cano, K. Abraham, H. Xandri-Monje, A. B. Cook, M. Hartlieb, F. Lévi, R. Dallmann, S. Perrier*

RAFT emulsion polymerisation as a platform to generate well-defined biocompatible latex nanoparticles